

Distance Priors from Planck and Dark Energy Constraints from Current Data

Yun Wang^{1*}, Shuang Wang^{1,2}¹*Homer L. Dodge Department of Physics & Astronomy,**Univ. of Oklahoma, 440 W Brooks St., Norman, OK 73019*²*Department of Physics, College of Sciences, Northeastern University, Shenyang 110004, China*

We derive distance priors from Planck first data release, and examine their impact on dark energy constraints from current observational data. We give the mean values and covariance matrix of $\{R, l_a, \Omega_b h^2, n_s\}$, which give an efficient summary of Planck data. The CMB shift parameters are $R = \sqrt{\Omega_m H_0^2} r(z_*)$, and $l_a = \pi r(z_*)/r_s(z_*)$, where z_* is the redshift at the last scattering surface, and $r(z_*)$ and $r_s(z_*)$ denote our comoving distance to z_* and sound horizon at z_* respectively.

We find that Planck distance priors are significantly tighter than those from WMAP9. However, adding Planck distance priors does not lead to significantly improved dark energy constraints using current data, compared to adding WMAP9 distance priors. This is because Planck data appear to favor a higher matter density and lower Hubble constant, in tension with most of the other current cosmological data sets. Adding Planck distance priors to current data leads to a marginal inconsistency with a cosmological constant in a flat universe.

PACS numbers: 98.80.Es, 98.80.-k, 98.80.Jk

Keywords: Cosmology

I. INTRODUCTION

Current observational data do not yet allow us to differentiate two likely explanations for the observed cosmic acceleration [1, 2]: dark energy, and the modification of general relativity. For recent reviews, see [3–11]. Cosmic acceleration is generally referred to as “dark energy” for convenience.

There are three vigorously studied direct probes of dark energy. Type Ia supernovae (SNe Ia) probe the Hubble parameter $H(z)$ (i.e., the expansion history of the universe) via the measurement of luminosity distances to the SNe Ia [1, 2]. Galaxy clustering (GC) directly probes $H(z)$ (and its integral form $D_A(z)$) via the baryon acoustic oscillation (BAO) [12, 13] measurements, and the growth rate $f_g(z)$ (i.e., the growth history of cosmic large scale structure) via redshift space distortion measurements. Weak lensing of galaxies probes a combination of the expansion history and growth history of the universe [14, 15].

While these direct probes of cosmic acceleration complement each other, each with its own set of systematic uncertainties, they require the inclusion of cosmic microwave background (CMB) anisotropy data to help break the degeneracies among the dark energy and cosmological parameters. This is because CMB data provide the strongest constraints on cosmological parameters (see, e.g., [16]).

Direct measurements of the Hubble constant (see, e.g., [17]) also help break the degeneracy amongst the dark energy and cosmological parameters. Other data, e.g.,

gamma ray bursts [18–20], can help strengthen the dark energy constraints.

In this paper, we derive distance priors from the Planck first data release, and examine their impact on dark energy constraints from current observational data.

We describe our method in Sec.II, present our results in Sec.III, and conclude in Sec.IV.

II. METHOD

Our main goal is to derive distance priors from Planck data, and illustrate their impact on current observational data. For simplicity and clarity, we only use methods that give geometric constraints on dark energy in this paper. The constraints on the growth rate of cosmic large scale structure are degenerate with the geometric constraints (see, e.g., [21, 22]). We adopt a conservative approach by marginalizing over the growth constraints.

Geometric constraints on dark energy are derived from the measurement of distances. The comoving distance to an object at redshift z is given by:

$$r(z) = cH_0^{-1} |\Omega_k|^{-1/2} \text{sinn}[|\Omega_k|^{1/2} \Gamma(z)] \quad (1)$$

$$\Gamma(z) = \int_0^z \frac{dz'}{E(z')}, \quad E(z) = H(z)/H_0$$

where $\text{sinn}(x) = \sin(x)$, x , $\sinh(x)$ for $\Omega_k < 0$, $\Omega_k = 0$, and $\Omega_k > 0$ respectively; and the expansion rate of the universe $H(z)$ (i.e., the Hubble parameter) is given by

$$H^2(z) \equiv \left(\frac{\dot{a}}{a}\right)^2 \quad (2)$$

$$= H_0^2 [\Omega_m(1+z)^3 + \Omega_r(1+z)^4 + \Omega_k(1+z)^2 + \Omega_X X(z)],$$

*email: wang@nhn.ou.edu

where $\Omega_m + \Omega_r + \Omega_k + \Omega_X = 1$, Ω_m includes the contribution from massive neutrinos, and the dark energy density function $X(z)$ is defined as

$$X(z) \equiv \frac{\rho_X(z)}{\rho_X(0)}. \quad (3)$$

Note that $\Omega_r = \Omega_m/(1 + z_{\text{eq}}) \ll \Omega_m$ (with z_{eq} denoting the redshift at matter-radiation equality), thus the Ω_r term is usually omitted in dark energy studies at $z \ll 1000$, since dark energy should only be important at late times.

A. CMB data

CMB data give us the comoving distance to the photon-decoupling surface $r(z_*)$, and the comoving sound horizon at photon-decoupling epoch $r_s(z_*)$ [23]. Wang & Mukherjee (2007) [24] showed that the CMB shift parameters

$$\begin{aligned} R &\equiv \sqrt{\Omega_m H_0^2} r(z_*)/c, \\ l_a &\equiv \pi r(z_*)/r_s(z_*), \end{aligned} \quad (4)$$

together with $\omega_b \equiv \Omega_b h^2$, provide an efficient summary of CMB data as far as dark energy constraints go. This has been verified by [25]. Replacing ω_b with z_* gives identical constraints when the CMB distance priors are combined with other data [26]. Using ω_b , instead of z_* , is more appropriate in an MCMC analysis in which ω_b is a base parameter.

Note that in order to summarize the CMB data, R and l_a are defined to contain the physical parameters $\Omega_m h^2$ (matter density), $r(z_*)$ (comoving distance to the photon-decoupling surface), and $\theta_* \propto l_a$ (angular size of the comoving sound horizon at photon-decoupling epoch), as these physical parameters are tightly constrained by CMB data and are essentially independent of model assumptions (except for the assumption on the cosmic curvature).

An intuitive explanation for the effectiveness of (R, l_a) in summarizing CMB data is as follows. As indicated by the detailed studies in Wang & Mukherjee (2007) [24], both R and l_a must be used to describe the complex degeneracies amongst the cosmological parameters that determine the CMB angular power spectrum. Models that correspond to the same value of R but different values of l_a give rise to very different CMB angular power spectra, because l_a determines the average acoustic peak structure. Models that correspond to the same value of l_a but different values of R have the same acoustic peak structure in their CMB angular power spectra, but the overall amplitude of the acoustic peaks is different in each model because of the difference in R . The inclusion of CMB lensing data in deriving the shift parameters makes little difference in their mean values, since the bulk of the information comes from the CMB angular power spectra,

but it does reduce their uncertainties by reducing parameter degeneracies.

The comoving sound horizon at redshift z is given by

$$\begin{aligned} r_s(z) &= \int_0^z \frac{c_s dt'}{a} = cH_0^{-1} \int_z^\infty dz' \frac{c_s}{E(z')}, \\ &= cH_0^{-1} \int_0^a \frac{da'}{\sqrt{3(1 + \bar{R}_b a') a'^4 E^2(z')}}}, \end{aligned} \quad (5)$$

where a is the cosmic scale factor, $a = 1/(1 + z)$, and $a^4 E^2(z) = \Omega_m(a + a_{\text{eq}}) + \Omega_k a^2 + \Omega_X X(z) a^4$, with $a_{\text{eq}} = \Omega_{\text{rad}}/\Omega_m = 1/(1 + z_{\text{eq}})$, and $z_{\text{eq}} = 2.5 \times 10^4 \Omega_m h^2 (T_{\text{CMB}}/2.7 \text{ K})^{-4}$. The sound speed is $c_s = 1/\sqrt{3(1 + \bar{R}_b a)}$, with $\bar{R}_b a = 3\rho_b/(4\rho_\gamma)$, $\bar{R}_b = 31500\Omega_b h^2 (T_{\text{CMB}}/2.7 \text{ K})^{-4}$. We take $T_{\text{CMB}} = 2.7255$.

The redshift to the photon-decoupling surface, z_* , is given by the fitting formula [27]:

$$z_* = 1048 [1 + 0.00124(\Omega_b h^2)^{-0.738}] [1 + g_1(\Omega_m h^2)^{g_2}], \quad (6)$$

where

$$g_1 = \frac{0.0783 (\Omega_b h^2)^{-0.238}}{1 + 39.5 (\Omega_b h^2)^{0.763}} \quad (7)$$

$$g_2 = \frac{0.560}{1 + 21.1 (\Omega_b h^2)^{1.81}} \quad (8)$$

The redshift of the drag epoch z_d is well approximated by [28]

$$z_d = \frac{1291(\Omega_m h^2)^{0.251}}{1 + 0.659(\Omega_m h^2)^{0.828}} [1 + b_1(\Omega_b h^2)^{b_2}], \quad (9)$$

where

$$b_1 = 0.313(\Omega_m h^2)^{-0.419} [1 + 0.607(\Omega_m h^2)^{0.674}] \quad (10)$$

$$b_2 = 0.238(\Omega_m h^2)^{0.223}. \quad (11)$$

Figs.1-4 show the one-dimensional marginalized probability distributions (pdf) of (l_a, R, ω_b, n_s) from Planck [29], WMAP9 [30], and WMAP7 [16] data, for $w_X(z) = -1$ and one massive neutrino (with mass of 0.06eV), and without assuming a flat universe. We have used the Planck archiv data to obtain constraints on (l_a, R, ω_b, n_s) from Planck and WMAP9; this archiv does not include $w_X(z) \neq -1$ cases without assuming a flat universe. Fortunately, the constraints on (l_a, R, ω_b, n_s) (including the pdf's) are *not* sensitive to the assumption about dark energy [31]. Three sets of pdf's are shown in Figs.1-4:

- (1) Planck+lensing+WP: Planck temperature data combined with Planck lensing, as well as WMAP polarization at low multipoles ($l \leq 23$). This set represents the tightest constraints from CMB data only at present. Note that excluding the Planck lensing data changes the mean values of (l_a, R, ω_b, n_s) by 0.2% or less, and increases the dispersions slightly.
- (2) WMAP: WMAP 9 year temperature and polarization

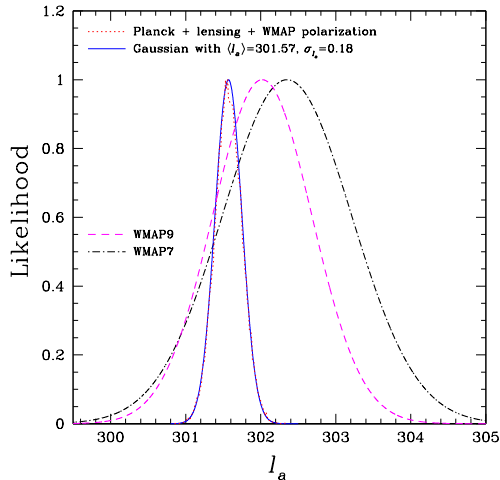


FIG. 1: One-dimensional marginalized probability distributions of CMB shift parameter l_a derived from Planck, WMAP9, and WMAP7 data.

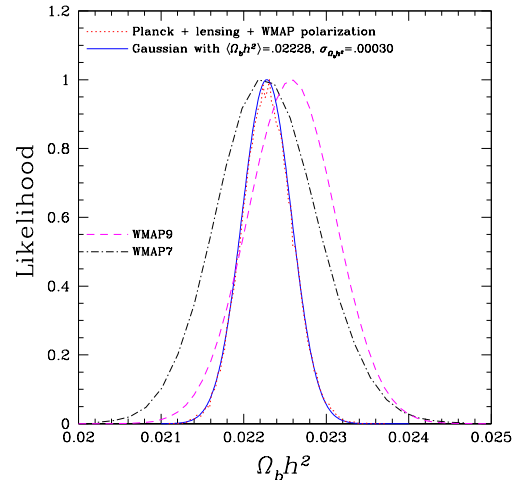


FIG. 3: One-dimensional marginalized probability distribution of the dimensionless baryon density, $\omega_b \equiv \Omega_b h^2$, derived from Planck, WMAP9, and WMAP7 data.

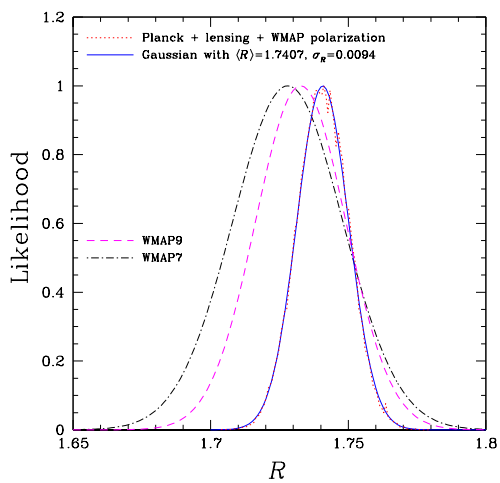


FIG. 2: One-dimensional marginalized probability distribution of CMB shift parameter R derived from Planck, WMAP9, and WMAP7 data.

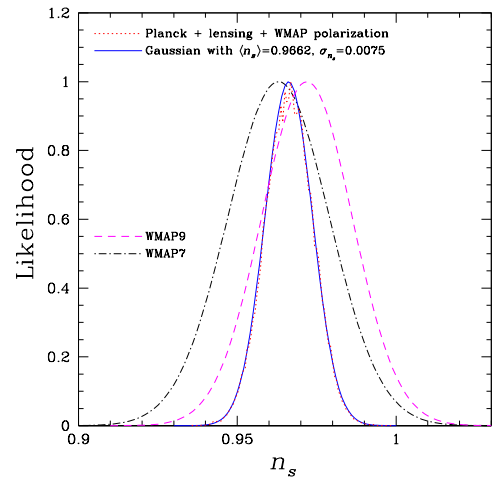


FIG. 4: One-dimensional marginalized probability distributions of powerlaw index of primordial matter power spectrum, n_s , derived from Planck, WMAP9, and WMAP7 data.

data.

(3) WMAP7: WMAP 7 year temperature and polarization data.

The Planck+lensing+WP pdf's in Figs.1-4 are well fitted by Gaussian distributions with the following means and standard deviations:

$$\begin{aligned}
 \langle l_a \rangle &= 301.57, \sigma(l_a) = 0.18 \\
 \langle R \rangle &= 1.7407, \sigma(R) = 0.0094 \\
 \langle \omega_b \rangle &= 0.02228, \sigma(\omega_b) = 0.00030 \\
 \langle n_s \rangle &= 0.9662, \sigma(n_s) = 0.0075.
 \end{aligned} \tag{12}$$

The normalized covariance matrix of (l_a, R, ω_b, n_s) is

$$\begin{pmatrix}
 1.0000 & 0.5250 & -0.4235 & -0.4475 \\
 0.5250 & 1.0000 & -0.6925 & -0.8240 \\
 -0.4235 & -0.6925 & 1.0000 & 0.6109 \\
 -0.4475 & -0.8240 & 0.6109 & 1.0000
 \end{pmatrix} \tag{13}$$

For comparison, we have also obtained the WMAP9 constraints on (l_a, R, ω_b, n_s) . The WMAP9 in Figs.1-4 are well fitted by Gaussian distributions with the following means and standard deviations:

$$\begin{aligned}
 \langle l_a \rangle &= 302.02, \sigma(l_a) = 0.66 \\
 \langle R \rangle &= 1.7327, \sigma(R) = 0.0164 \\
 \langle \omega_b \rangle &= 0.02260, \sigma(\omega_b) = 0.00053 \\
 \langle n_s \rangle &= 0.9719, \sigma(n_s) = 0.0143.
 \end{aligned} \tag{14}$$

The normalized covariance matrix of (l_a, R, ω_b, n_s) is

$$\begin{pmatrix} 1.0000 & 0.3883 & -0.6089 & -0.5391 \\ 0.3883 & 1.0000 & -0.5239 & -0.6523 \\ -0.6089 & -0.5239 & 1.0000 & 0.8563 \\ -0.5391 & -0.6523 & 0.8563 & 1.0000 \end{pmatrix} \quad (15)$$

The WMAP7 constraints are from [31].

Since the primary GC data we use in this paper have been marginalized over n_s [32], we should marginalize the CMB distance priors over n_s as well.¹ This means dropping the 4th row and 4th column from the normalized covariance matrix of (l_a, R, ω_b, n_s) , then obtain the covariance matrix for (l_a, R, ω_b) as follows:

$$\text{Cov}_{CMB}(p_i, p_j) = \sigma(p_i) \sigma(p_j) \text{NormCov}_{CMB}(p_i, p_j), \quad (16)$$

where $i, j = 1, 2, 3$. The rms variance $\sigma(p_i)$ and the normalized covariance matrix NormCov_{CMB} are given by Eqs.(12) and (13) for Planck+lensing+WP, and Eqs.(14) and (15) for WMAP9 respectively.

CMB data are included in our analysis by adding the following term to the χ^2 of a given model with $p_1 = l_a(z_*)$, $p_2 = R(z_*)$, and $p_3 = \omega_b$:

$$\chi_{CMB}^2 = \Delta p_i [\text{Cov}_{CMB}^{-1}(p_i, p_j)] \Delta p_j, \quad \Delta p_i = p_i - p_i^{data}, \quad (17)$$

where p_i^{data} are the mean from Eq.(12) and Eq.(14), and Cov_{CMB}^{-1} is the inverse of the covariance matrix of $[l_a(z_*), R(z_*), \omega_b]$ from Eq.(16). Note that $p_4 = n_s$ should be added if the constraints on n_s are included in the GC data.

B. Analysis of SN Ia Data

SN Ia data give measurements of the luminosity distance $d_L(z)$ through that of the distance modulus of each SN:

$$\mu_0 \equiv m - M = 5 \log \left[\frac{d_L(z)}{\text{Mpc}} \right] + 25, \quad (18)$$

where m and M represent the apparent and absolute magnitude of a SN. The luminosity distance $d_L(z) = (1+z)r(z)$, with the comoving distance $r(z)$ given by Eq.(1).

Care must be taken in interpreting supernova distances in an inhomogeneous universe [38]. We use the compilation of SN Ia data by Conley et al. (2011) [33], which include the SNe Ia from the first three years of the Supernova Legacy Survey (SNLS3), the largest homogeneous SN Ia data set publicly available at present, and apply flux-averaging to reduce the systematic bias due to weak

lensing magnification of SNe [34–36], as detailed in Wang, Chuang, & Mukherjee (2012) [31].

For a set of 472 SNe Ia, Conley et al. (2011) [33] give the apparent B magnitude, m_B , and the covariance matrix for $\Delta m \equiv m_B - m_{\text{mod}}$, with

$$m_{\text{mod}} = 5 \log_{10} \mathcal{D}_L(z|\mathbf{s}) - \alpha(s-1) + \beta\mathcal{C} + \mathcal{M}, \quad (19)$$

where $\mathcal{D}_L(z|\mathbf{s})$ is the luminosity distance multiplied by H_0 for a given set of cosmological parameters $\{\mathbf{s}\}$, s is the stretch measure of the SN light curve shape, and \mathcal{C} is the color measure for the SN. \mathcal{M} is a nuisance parameter representing some combination of the absolute magnitude of a fiducial SN Ia, M , and the Hubble constant H_0 . Since the time dilation part of the observed luminosity distance depends on the total redshift z_{hel} (special relativistic plus cosmological), we have [37]

$$\mathcal{D}_L(z|\mathbf{s}) \equiv c^{-1} H_0 (1+z_{\text{hel}}) r(z|\mathbf{s}), \quad (20)$$

where z and z_{hel} are the CMB restframe and heliocentric redshifts of the SN.

For a set of N SNe with correlated errors, we have [33]

$$\chi^2 = \Delta \mathbf{m}^T \cdot \mathbf{C}^{-1} \cdot \Delta \mathbf{m} \quad (21)$$

where $\Delta \mathbf{m}$ is a vector with N components, and \mathbf{C} is the $N \times N$ covariance matrix of the SNe Ia.

Note that Δm is equivalent to $\Delta \mu_0$, since

$$\Delta m \equiv m_B - m_{\text{mod}} = [m_B + \alpha(s-1) - \beta\mathcal{C}] - \mathcal{M}. \quad (22)$$

The total covariance matrix is [33]

$$\mathbf{C} = \mathbf{D}_{\text{stat}} + \mathbf{C}_{\text{stat}} + \mathbf{C}_{\text{sys}}, \quad (23)$$

with the diagonal part of the statistical uncertainty given by [33]

$$\begin{aligned} \mathbf{D}_{\text{stat},ii} &= \sigma_{m_B,i}^2 + \sigma_{\text{int}}^2 + \sigma_{\text{lensing}}^2 + \sigma_{\text{host correction}}^2 \\ &+ \left[\frac{5(1+z_i)}{z_i(1+z_i/2) \ln 10} \right]^2 \sigma_{z,i}^2 + \alpha^2 \sigma_{s,i}^2 + \beta^2 \sigma_{\mathcal{C},i}^2 \\ &+ 2\alpha C_{m_B s,i} - 2\beta C_{m_B \mathcal{C},i} - 2\alpha\beta C_{s \mathcal{C},i}, \end{aligned} \quad (24)$$

where $C_{m_B s,i}$, $C_{m_B \mathcal{C},i}$, and $C_{s \mathcal{C},i}$ are the covariances between m_B , s , and \mathcal{C} for the i -th SN. Note also that $\sigma_{z,i}^2$ includes a peculiar velocity residual of 0.0005 (i.e., 150 km/s) added in quadrature [33].

The statistical and systematic covariance matrices, \mathbf{C}_{stat} and \mathbf{C}_{sys} , are generally not diagonal [33], and are given in the form:

$$\mathbf{C}_{\text{stat}} + \mathbf{C}_{\text{sys}} = V_0 + \alpha^2 V_a + \beta^2 V_b + 2\alpha V_{0a} - 2\beta V_{0b} - 2\alpha\beta V_{ab}. \quad (25)$$

where V_0 , V_a , V_b , V_{0a} , V_{0b} , and V_{ab} are matrices given by the SNLS data archive at <https://tspace.library.utoronto.ca/handle/1807/24512/>. \mathbf{C}_{stat} includes the uncertainty in the SN model. \mathbf{C}_{sys} includes the uncertainty in the zero point. Note that

¹ An improved approach is to use GC data that retain the n_s dependence, and combine with the CMB constraints on (l_a, R, ω_b, n_s) .

\mathbf{C}_{stat} and \mathbf{C}_{sys} do not depend on \mathcal{M} , since the relative distance moduli are independent of the value of \mathcal{M} [33].

We refer the reader to Conley et al. (2011) [33] for a detailed discussion of the origins of the statistical and systematic errors. As an example, we note that the correlation of errors on different SNe arises from a statistical uncertainty in the zero point of one passband, e.g., r_M . This directly affects all SNe with r_M measurements due to K-corrections (restframe B to r_M), and indirectly affects even the SNe without r_M measurements through the empirical SN models by changing the templates and the measured color-luminosity relationship.

For χ^2 statistics using MCMC or a grid of parameters, here are the steps in flux-averaging [31]:

(1) Convert the distance modulus of SNe Ia into “fluxes”,

$$F(z_l) \equiv 10^{-(\mu_0^{\text{data}}(z_l) - 25)/2.5} = \left(\frac{d_L^{\text{data}}(z_l)}{\text{Mpc}} \right)^{-2}. \quad (26)$$

(2) For a given set of cosmological parameters $\{\mathbf{s}\}$, obtain “absolute luminosities”, $\{\mathcal{L}(z_l)\}$, by removing the redshift dependence of the “fluxes”, i.e.,

$$\mathcal{L}(z_l) \equiv d_L^2(z_l|\mathbf{s}) F(z_l). \quad (27)$$

(3) Flux-average the “absolute luminosities” $\{\mathcal{L}_l^i\}$ in each redshift bin i to obtain $\{\bar{\mathcal{L}}^i\}$:

$$\bar{\mathcal{L}}^i = \frac{1}{N_i} \sum_{l=1}^{N_i} \mathcal{L}_l^i(z_l^{(i)}), \quad \bar{z}_i = \frac{1}{N_i} \sum_{l=1}^{N_i} z_l^{(i)}. \quad (28)$$

(4) Place $\bar{\mathcal{L}}^i$ at the mean redshift \bar{z}_i of the i -th redshift bin, now the binned flux is

$$\bar{F}(\bar{z}_i) = \bar{\mathcal{L}}^i / d_L^2(\bar{z}_i|\mathbf{s}). \quad (29)$$

(5) Compute the covariance matrix of $\bar{F}(\bar{z}_i)$ and $\bar{F}(\bar{z}_j)$:

$$\begin{aligned} & \text{Cov} [\bar{F}(\bar{z}_i), \bar{F}(\bar{z}_j)] \\ &= \frac{1}{N_i N_j} \left[\frac{\ln 10 / 2.5}{d_L(\bar{z}_i|\mathbf{s}) d_L(\bar{z}_j|\mathbf{s})} \right]^2 \\ & \sum_{l=1}^{N_i} \sum_{m=1}^{N_j} \mathcal{L}(z_l^{(i)}) \mathcal{L}(z_m^{(j)}) \langle \Delta\mu_0^{\text{data}}(z_l^{(i)}) \Delta\mu_0^{\text{data}}(z_m^{(j)}) \rangle \end{aligned} \quad (30)$$

where $\langle \Delta\mu_0^{\text{data}}(z_l^{(i)}) \Delta\mu_0^{\text{data}}(z_m^{(j)}) \rangle$ is the covariance of the measured distance moduli of the l -th SN Ia in the i -th redshift bin, and the m -th SN Ia in the j -th redshift bin. $\mathcal{L}(z)$ is defined by Eqs.(26) and (27).

(6) For the flux-averaged data, $\{\bar{F}(\bar{z}_i)\}$, compute

$$\chi^2 = \sum_{ij} \Delta\bar{F}(\bar{z}_i) \text{Cov}^{-1} [\bar{F}(\bar{z}_i), \bar{F}(\bar{z}_j)] \Delta\bar{F}(\bar{z}_j) \quad (31)$$

where

$$\Delta\bar{F}(\bar{z}_i) \equiv \bar{F}(\bar{z}_i) - F^p(\bar{z}_i|\mathbf{s}), \quad (32)$$

with $F^p(\bar{z}_i|\mathbf{s}) = (d_L(z|\mathbf{s})/\text{Mpc})^{-2}$.

For the sample of SNe we use in this study, we flux-averaged the SNe with $dz = 0.04$, to ensure that almost all redshift bins contain at least one SN. Our SN flux-averaging code is available at <http://www.nhn.ou.edu/~wang/SNcode/>.

C. Galaxy Clustering Data

For GC data, we use the measurements of $H(z)r_s(z_d)/c$ and $D_A(z)/r_s(z_d)$ (where $H(z)$ is the Hubble parameter, $D_A(z)$ is the angular diameter distance, and $r_s(z_d)$ is the sound horizon at the drag epoch) from the two-dimensional two-point correlation function measured at $z=0.35$ [32] and $z=0.57$ [39]. The $z = 0.35$ measurement was made by Chuang & Wang (2012) [32] using a sample of the SDSS DR7 Luminous Red Galaxies (LRGs). The $z = 0.57$ measurement was made by Chuang et al. (2013) [39] using the CMASS galaxy sample from BOSS.

Using the two-dimensional two-point correlation function of SDSS DR7 in the scale range of 40-120 Mpc/ h , Chuang & Wang (2012) [32] found that

$$\begin{aligned} H(z = 0.35)r_s(z_d)/c &= 0.0434 \pm 0.0018 \\ D_A(z = 0.35)/r_s(z_d) &= 6.60 \pm 0.26 \\ r &= 0.0604 \end{aligned} \quad (33)$$

where r is the normalized correlation coefficient between $H(z = 0.35)r_s(z_d)/c$ and $D_A(z = 0.35)/r_s(z_d)$, and $r_s(z_d)$ is the sound horizon at the drag epoch (given by Eqs.(5) and (9)).

In a similar analysis using the CMASS galaxy sample from BOSS, Chuang et al. (2013) found that

$$\begin{aligned} H(z = 0.57)r_s(z_d)/c &= 0.0454 \pm 0.0031 \\ D_A(z = 0.57)/r_s(z_d) &= 8.95 \pm 0.27 \\ r &= 0.4874 \end{aligned} \quad (34)$$

We marginalize over the growth rate measurement made by Chuang et al. 2013 [39] for a conservative approach.

GC data are included in our analysis by adding $\chi_{GC}^2 = \chi_{GC1}^2 + \chi_{GC2}^2$, with $z_{GC1} = 0.35$ and $z_{GC2} = 0.57$, to the χ^2 of a given model. Note that

$$\chi_{GCi}^2 = \Delta p_i [C_{GC}^{-1}(p_i, p_j)] \Delta p_j, \quad \Delta p_i = p_i - p_i^{\text{data}}, \quad (35)$$

where $p_1 = H(z_{GCi})r_s(z_d)/c$ and $p_2 = D_A(z_{GCi})/r_s(z_d)$, with $i = 1, 2$.

D. Gammay-ray Burst Data

We add gammay-ray burst (GRB) data to our analysis, since these are complementary in redshift range to the SN Ia data. We use GRB data in the form of the model-independent GRB distance measurements from Wang

(2008c) [40], which were derived from the data of 69 GRBs with $0.17 \leq z \leq 6.6$ from Schaefer (2007) [41]².

The GRB distance measurements are given in terms of [40]

$$\bar{r}_p(z_i) \equiv \frac{r_p(z)}{r_p(0.17)}, \quad r_p(z) \equiv \frac{(1+z)^{1/2}}{z} \frac{H_0}{ch} r(z), \quad (36)$$

where $r(z)$ is the comoving distance at z .

The GRB data are included in our analysis by adding the following term to the χ^2 of a given model:

$$\chi_{GRB}^2 = [\Delta \bar{r}_p(z_i)] \cdot (\text{Cov}_{GRB}^{-1})_{ij} \cdot [\Delta \bar{r}_p(z_j)]$$

$$\Delta \bar{r}_p(z_i) = \bar{r}_p^{\text{data}}(z_i) - \bar{r}_p(z_i), \quad (37)$$

where $\bar{r}_p(z)$ is defined by Eq.(36). The covariance matrix is given by

$$(\text{Cov}_{GRB})_{ij} = \sigma(\bar{r}_p(z_i))\sigma(\bar{r}_p(z_j)) (\overline{\text{Cov}}_{GRB})_{ij}, \quad (38)$$

where $\overline{\text{Cov}}_{GRB}$ is the normalized covariance matrix from Table 3 of Wang (2008c) [40], and

$$\sigma(\bar{r}_p(z_i)) = \sigma(\bar{r}_p(z_i))^+, \quad \text{if } \bar{r}_p(z) \geq \bar{r}_p(z)^{\text{data}},$$

$$\sigma(\bar{r}_p(z_i)) = \sigma(\bar{r}_p(z_i))^- , \quad \text{if } \bar{r}_p(z) < \bar{r}_p(z)^{\text{data}}, \quad (39)$$

where $\sigma(\bar{r}_p(z_i))^+$ and $\sigma(\bar{r}_p(z_i))^-$ are the 68% C.L. errors given in Table 2 of Wang (2008c) [40].

E. Dark energy parametrization

Since we are ignorant of the true nature of dark energy, it is useful to measure the dark energy density function $X(z) \equiv \rho_X(z)/\rho_X(0)$ as a free function of redshift [46–48]. This has the advantage of allowing dark energy models in which $\rho_X(z)$ becomes negative in the future, e.g., the “Big Crunch” models [49, 50], which are precluded if we parametrize dark energy with an equation of state $w_X(z)$ [47].

Here we parametrize $X(z)$ by cubic-splining its values at $z = 1/3, 2/3$, and 1.0 , and assume that $X(z > 1) = X(z = 1)$. For simplicity of notation, we define $X_{0.33} \equiv X(z = 1/3)$, $X_{0.67} \equiv X(z = 2/3)$, and $X_{1.0} \equiv X(z = 1)$. Fixing $X(z > 1)$ reflects the limit of current data, and avoids making assumptions about early dark energy that can be propagated into artificial constraints on dark energy at low z [24, 47].

For comparison with the work of others, we also consider a dark energy equation of state linear in the cosmic scale factor a , $w_X(a) = w_0 + (1 - a)w_a$ [51]. A related parametrization is [26]

$$w_X(z) = w_0(3a - 2) + 3w_{0.5}(1 - a), \quad (40)$$

where $w_{0.5} \equiv w_X(z = 0.5)$. Wang (2008b) [26] showed that $(w_0, w_{0.5})$ are much less correlated than (w_0, w_a) , thus are a better set of parameters to use. We find that $(w_0, w_{0.5})$ converge much faster than (w_0, w_a) in a Markov Chain Monte Carlo (MCMC) likelihood analysis for the same data.

III. RESULTS

We perform a MCMC likelihood analysis [52] to obtain $\mathcal{O}(10^6)$ samples for each set of results presented in this paper. We assume flat priors for all the parameters, and allow ranges of the parameters wide enough such that further increasing the allowed ranges has no impact on the results. We process the MCMC chains following the standard practice of ensuring convergence and thinning using CosmoMC.

In addition to the SN Ia, CMB, GC, and GRB data discussed in Sec.II, we impose a prior of $H_0 = 73.8 \pm 2.4 \text{ km s}^{-1} \text{ Mpc}^{-1}$, from the HST measurements by Riess et al. (2011) [17].

We do *not* assume a flat universe. In addition to the dark energy parameters described in Sec.IIE, we also constrain cosmological parameters $(\Omega_m, \Omega_k, h, \omega_b)$, where $\omega_b \equiv \Omega_b h^2$. In addition, we marginalize over the SN Ia nuisance parameters $\{\alpha, \beta, \mathcal{M}\}$. We only use flux-averaged SN Ia data (with $dz = 0.04$), as flux-averaging reduces the impact of systematic uncertainties on dark energy and cosmological parameter constraints [31].

We will present results for dark energy density at $z = 1/3, 2/3$, and 1 , as well as (w_0, w_a) and $(w_0, w_{0.5})$, and a constant dark energy equation of state w .

A. Constraints on dark energy density function $X(z)$

Figs.5-8 summarize our constraints on $X(z)$ parametrized by its value at $z = 1/3, 2/3$, and 1 . Planck data give very similar results as WMAP9 data on $X(z)$, even although Planck data favor higher Ω_m . However, note that adding Planck priors leads to a marginal inconsistency with a cosmological constant in a flat universe (see bottom right panel in Fig.6).

Adding BOSS data has a more significant impact: it shifts the value of $X_{0.67}$ away from 1 at $\sim 1.5\sigma$ (see Fig.6 and Fig.8), independent of cosmic curvature.

B. Constraints on a linear dark energy equation of state

We have studied the constraints on both (w_0, w_a) and $(w_0, w_{0.5})$, as these have different base parameters (assumed to have flat priors). In order to compare with previous work, and to display the impact of replacing

² The proper calibration of GRBs is an active area of research. For recent studies on the impact of detector thresholds, spectral analysis, and unknown selection effects, see, e.g., [42–45].

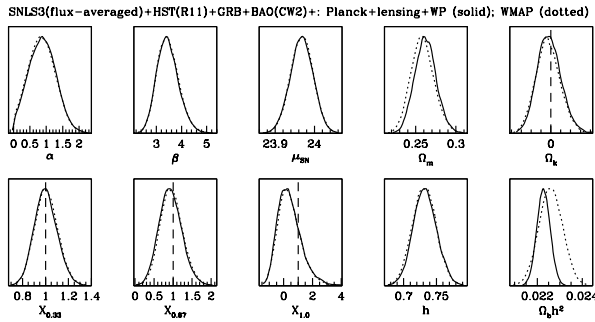


FIG. 5: The marginalized probability distributions for $\{X_{0.33}, X_{0.67}, X_{1.0}, \Omega_m, \Omega_k, h, \omega_b, \alpha, \beta, \mathcal{M}\}$, for SNe+ H_0 +GRB+GC(CW12), combined with Planck+lensing+WP (solid) and WMAP9 (dotted) data respectively.

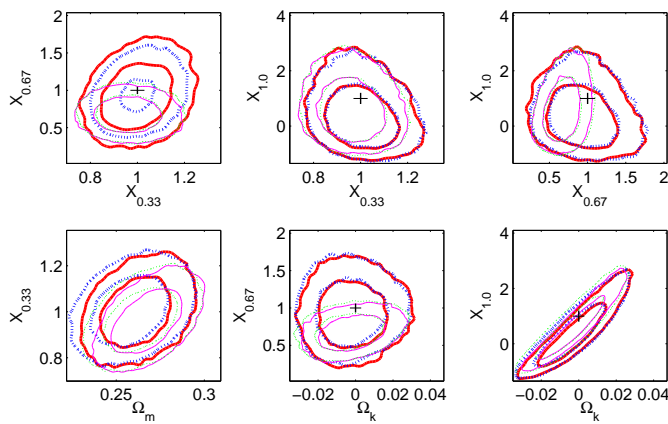


FIG. 6: The joint 68% and 95% confidence contours for parameters of interest for SNe+ H_0 +GRB+GC(CW12), combined with Planck+lensing+WP (solid) and WMAP9 (dotted) data respectively. The thin solid and dotted contours also include GC data from BOSS.

WMAP9 priors with Planck+lensing+WP priors, we do not include GC data from BOSS in this comparison.

Fig.9 shows the joint 68% and 95% confidence contours for (w_0, w_a) (left panel) and $(w_0, w_{0.5})$ (right panel), for SNe+ H_0 +GRB+GC(CW12), combined with Planck+lensing+WP (solid) and WMAP9 (dotted) data respectively. Fig.10 shows the corresponding joint 68% and 95% confidence contours for (Ω_k, w_a) (left panel) and $(\Omega_k, w_{0.5})$ (right panel), for the same data and with the same line types. Fig.9 indicates that Planck priors do not have a significant impact on the constraints on a linear dark energy equation state; this means that the DETF FoM remains approximately the same compared to that found by [31] using WMAP7 priors (using WMAP9 priors gives similar results as using WMAP7 priors). It is interesting to note that the right panel of Fig.10 shows that the combined data with Planck priors rule out $w_{0.5} = -1$ and a flat universe at $\sim 1.5\sigma$. Planck data favor a small but positive Ω_k (i.e., a slightly open universe).

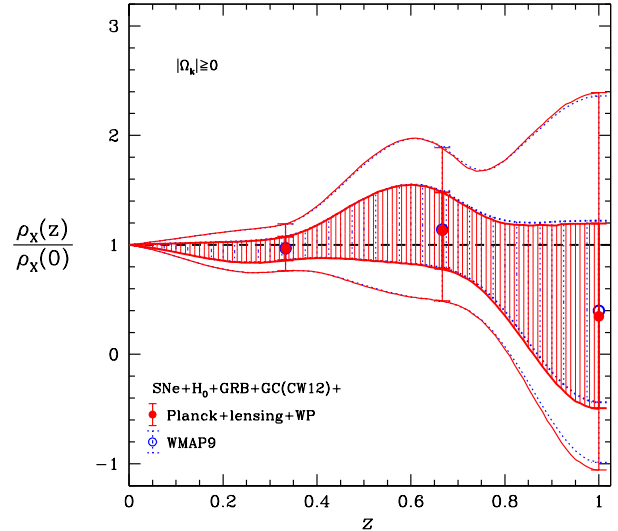


FIG. 7: The 68% and 95% confidence constraints for $X(z)$ (cubic-splined from $\{X_{0.33}, X_{0.67}, X_{1.0}\}$), for SNe+ H_0 +GRB+GC(CW12), combined with Planck+lensing+WP (solid) and WMAP9 (dotted) data respectively.

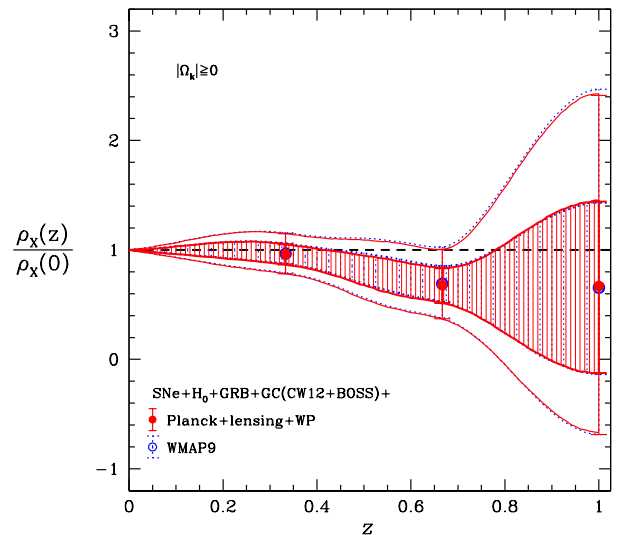


FIG. 8: The 68% and 95% confidence constraints for $X(z)$ (cubic-splined from $\{X_{0.33}, X_{0.67}, X_{1.0}\}$), for SNe+ H_0 +GRB+GC(CW12+BOSS), combined with Planck+lensing+WP (solid) and WMAP9 (dotted) data respectively.

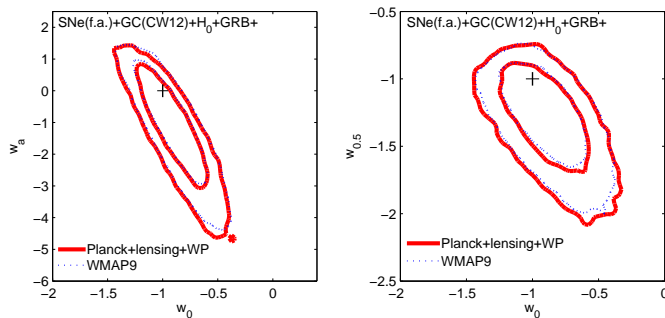


FIG. 9: The joint 68% and 95% confidence contours for (w_0, w_a) (left panel) and $(w_0, w_{0.5})$ (right panel), for SNe+ H_0 +GRB+GC(CW12), combined with Planck+lensing+WP (solid) and WMAP9 (dotted) data respectively.

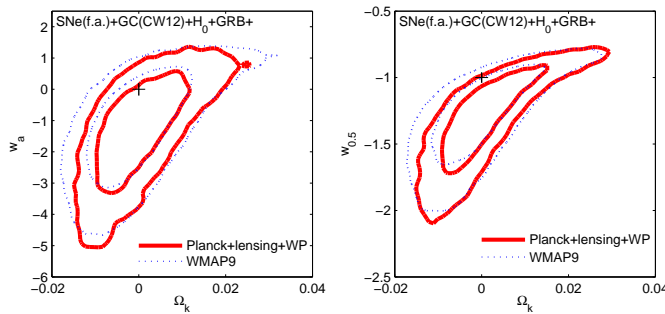


FIG. 10: The joint 68% and 95% confidence contours for (Ω_k, w_a) (left panel) and $(\Omega_k, w_{0.5})$ (right panel), for SNe+ H_0 +GRB+GC(CW12), combined with Planck+lensing+WP (solid) and WMAP9 (dotted) data respectively.

C. Constraints on a constant dark energy equation of state

In order to understand better the difference between the Planck+lensing+WP priors and the WMAP9 priors, we now study a constant dark energy equation of state, for the minimal combination of SNe+ H_0 data with the CMB priors.

Fig.11 shows the joint 68% and 95% confidence contours for (Ω_k, w) (left panel) and (Ω_m, w) (right panel), for SNe+ H_0 , combined with Planck+lensing+WP (solid) and WMAP9 (dotted) data respectively. Here, we see even more clearly the trend of Planck+lensing+WP priors favoring a small but positive Ω_k (a slightly open universe), and a somewhat higher Ω_m , compared to WMAP9 priors. Again, we find that adding Planck priors to other data leads to a marginal inconsistency with a cosmological constant in a flat universe.

IV. DISCUSSION AND SUMMARY

We have derived the distance priors from Planck first data release, in the form of the mean values and covariance matrix of $\{R, l_a, \Omega_b h^2, n_s\}$, which give an ef-

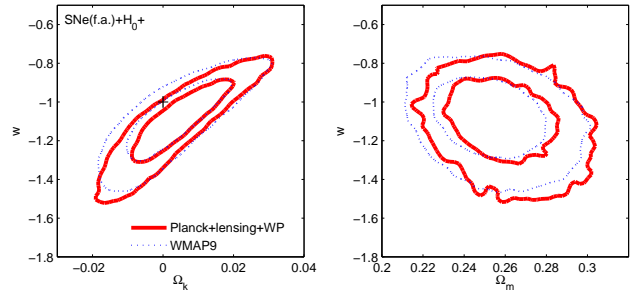


FIG. 11: The joint 68% and 95% confidence contours for (Ω_k, w) (left panel) and (Ω_m, w) (right panel), for SNe+ H_0 , combined with Planck+lensing+WP (solid) and WMAP9 (dotted) data respectively.

ficient summary of Planck data in the context of dark energy constraints. As a test of the accuracy of this approach, we compare the constraints on a constant dark energy equation of state w in a flat universe using Planck+lensing+WP data combined with SNLS SNe (no flux-averaging) in the form of MCMC chains from the Planck data archiv, with the Planck+lensing+WP data summarized by $\{R, l_a, \Omega_b h^2\}$ combined with the same SN data. We find $w = -1.10 (-1.18, -1.02)$ for Planck+lensing+WP data summarized by $\{R, l_a, \Omega_b h^2\}$, in excellent agreement with $w = -1.12 (-1.18, -1.05)$ from the full Planck+lensing+WP data. Not surprisingly, the full CMB data give slightly tighter constraints, but the difference is not statistically significant.

We have used constraints on $\{R, l_a, \Omega_b h^2\}$ from Planck data in combination with other data to probe dark energy in a conservative geometric approach. We have considered three different dark energy parametrizations: (1) Dark energy density $X(z) = \rho_X(z)/\rho_X(0)$, parametrized by splining its values at $z = 1/3, 2/3$, and 1.0. (2) Dark energy equation of state linear in the cosmic scale factor, $w_X(z) = w_0 + w_a(1-a)$, as well as the alternative parametrization with much less correlated parameters w_0 and $w_{0.5}$, $w_X(z) = w_0(3a-2) + 3w_{0.5}(1-a)$. (3) Constant dark energy equation of state $w_X(z) = w$.

In addition to CMB priors, we used SNe compiled by Conley et al. (2011) [33], flux-averaged to reduce systematic errors, the Hubble constant measurement by Riess et al. (2011) [17], the GRB data as summarized in Wang (2008) [40], and GC data from SDSS DR7 derived by Chuang & Wang (2012) [32]. We have chosen to use the same data as in [31], except for the CMB priors (Planck+lensing+WP and WMAP9, versus WMAP7), in order to compare the impact of the various CMB priors. For completeness, we have added the GC data from BOSS derived by Chuang et al. (2013) [39] in constraining $X(z)$.

We find that when dark energy density is allowed to be a free function, current data (excluding GC data from BOSS, with either Planck+lensing+WP or WMAP pri-

ors) are fully consistent with a cosmological constant and a flat universe at 95% C.L., but deviate from a cosmological constant in a flat universe at $\sim 68\%$ C.L. (see Fig.6). The addition of BOSS data leads to a deviation from a cosmological constant at the redshift near that of the BOSS data at $> 68\%$ confidence independent of cosmic curvature (see Fig.6). In general, adding Planck+lensing+WP priors leads to a preference for a small positive Ω_k (i.e., a slightly open universe) for a cosmological constant, or a flat universe with dark energy deviating from a cosmological constant, compared to adding WMAP9 priors (see Fig.6).

When dark energy equation of state is assumed to be a linear function in the cosmic scale factor $a(t)$, the dark energy constraints depend on the base parameters used, the highly correlated $\{w_0, w_a\}$, or the much less correlated $\{w_0, w_{0.5}\}$. The constraints on $\{w_0, w_a\}$ are consistent with a cosmological constant and a flat universe for both Planck+lensing+WP and WMAP9 priors, while that on $\{w_0, w_{0.5}\}$ are marginally inconsistent with a cosmological constant in a flat universe (see Fig.9 and Fig.10) for Planck+lensing+WP priors, similar to our findings in the $X(z)$ case.

We find that the above trend in the Planck+lensing+WP versus WMAP9 comparison becomes more pronounced when we assume a constant dark energy equation of state. Here we only

combine CMB priors with a minimal set of other data, SNe and H_0 , to highlight the difference between Planck+lensing+WP and WMAP9 priors. We find that adding the Planck+lensing+WP priors to the SNe and H_0 measurement leads to an inconsistency with a cosmological constant in a flat universe at $> 68\%$ confidence level (see Fig.11).

To conclude, we find that Planck distance priors are significantly tighter than those from WMAP9 (see Figs.1-3). However, adding Planck distance priors does not lead to significantly improved dark energy constraints using current data, compared to adding WMAP9 distance priors. This is because Planck data appear to favor a higher matter density and lower Hubble constant [29], in tension with most of the other current cosmological data sets.

In order to understand the nature of dark energy, we will need to improve our understanding of the systematic uncertainties of all data used. Future dark energy measurements from space [53–56] that minimize systematic uncertainties by design will enable us to make dramatic progress in our quest to shed light on dark energy.

Acknowledgments We acknowledge the use of Planck data archiv and CosmoMC. This work is supported in part by DOE grant DE-FG02-04ER41305.

-
- [1] Riess, A. G, *et al.*, 1998, *Astron. J.*, 116, 1009
[2] Perlmutter, S. *et al.*, 1999, *ApJ*, 517, 565
[3] Copeland, E. J., Sami, M., Tsujikawa, S., *IJMPD*, 15 (2006), 1753
[4] Ruiz-Lapuente, P., *Class. Quantum. Grav.*, 24 (2007), 91
[5] Ratra, B., Vogeley, M. S., arXiv:0706.1565 (2007)
[6] Frieman, J., Turner, M., Huterer, D., *ARAA*, 46, 385 (2008)
[7] Caldwell, R. R., & Kamionkowski, M., arXiv:0903.0866
[8] Uzan, J.-P., arXiv:0908.2243
[9] Wang, Y., *Dark Energy*, Wiley-VCH (2010)
[10] Li, M., *et al.*, 2011, arXiv:1103.5870
[11] Weinberg, D. H.; *et al.*, *Physics Reports*, in press, arXiv:1201.2434
[12] Blake, C.; Glazebrook, K., 2003, *ApJ*, 594, 665
[13] Seo, H; Eisenstein, D J 2003, *ApJ*, 598, 720
[14] Hu, W., 2002, *PRD*, 66, 083515
[15] Jain, B. & Taylor, A. *PRL*, 91, 141302 (2003)
[16] Komatsu, E., *et al.* 2011, *Astrophys.J.Suppl.*, 192, 18
[17] Riess, A. G, *et al.*, 2011, *ApJ*, 730, 119
[18] Amati, L., *et al.* 2002, *A&A*, 390, 81
[19] Bloom, J. S., Frail, D. A., & Kulkarni, S. R. 2003, *ApJ*, 594, 674
[20] Schaefer, B. E., 2003, *ApJ*, 583, L71
[21] Wang, Y., *Journal of Cosmology and Astroparticle Physics*, 05, 021 (2008).
[22] Simpson, F., & Peacock, J.A. 2010, *Phys Rev D*, 81, 043512
[23] Page, L., *et al.* 2003, *ApJS*, 148, 233
[24] Wang, Y., & Mukherjee, P., *PRD*, 76, 103533 (2007)
[25] Li, H., *et al.*, *ApJ*, 683, L1 (2008)
[26] Wang, Y., 2008b, *Phys. Rev. D* 77, 123525
[27] Hu, W., & Sugiyama, N. 1996, *ApJ*, 471, 542
[28] Eisenstein, D. & Hu, W. 1998, *ApJ*, 496, 605
[29] Ade, P. A. R., *et al.*, arXiv:1303.5076
[30] Bennett, C. L., *et al.*, arXiv:1212.5225
[31] Wang, Y.; Chuang, C.-H.; & Mukherjee, P., *Phys. Rev. D* 85, 023517 (2012)
[32] Chuang, C.-H.; and Wang, Y., *MNRAS*, 426, 226 (2012)
[33] Conley, A., *et al.*, 2011, *Astrophys.J.Suppl.*, 192, 1
[34] Wang, Y., *ApJ* 536, 531 (2000)
[35] Wang, Y., & Mukherjee, P. 2004, *ApJ*, 606, 654
[36] Wang, Y., *JCAP*, 03, 005 (2005)
[37] Hui, L., & Greene, P.B., *PRD*, 73, 123526 (2006)
[38] Clarkson, C., *et al.*, arXiv:1109.2484v2
[39] Chuang, C.H., *et al.*, arXiv:1303.4486
[40] Wang, Y., 2008b, *PRD*, 78, 123532
[41] Schaefer, B. E., 2007, *ApJ*, 660, 16
[42] Butler, N.R. *et al.*, *ApJ*, 2007,671, 656
[43] Butler, N.R. *et al.*, *ApJ*, 2009,694, 76
[44] Petrosian, V.; Bouvier, A.; Ryde, F., arXiv:0909.5051
[45] Shahmoradi, A., & Nemiroff, R.J., *MNRAS*, 2011,411, 1843
[46] Wang, Y., and Garnavich, P. 2001, *ApJ*, 552, 445
[47] Wang, Y., & Tegmark, M. 2004, *Phys. Rev. Lett.*, 92, 241302
[48] Wang, Y., & Freese, K. 2006, *Phys.Lett. B*632, 449 (astro-ph/0402208)
[49] Linde, A. D., "Inflation And Quantum Cosmology," in *Three hundred years of gravitation*, (Eds.: Hawking, S.W.

- and Israel, W., Cambridge Univ. Press, 1987), 604-630.
- [50] Wang, Y.; Kratochvil, J. M.; Linde, A.; & Shmakova, M., JCAP 0412 (2004) 006
- [51] Chevallier, M., & Polarski, D. 2001, Int. J. Mod. Phys. D10, 213
- [52] Lewis, A., & Bridle, S. 2002, PRD, 66, 103511
- [53] Crotts, A. et al., 2005, astro-ph/0507043
- [54] Cimatti, A., et al., Experimental Astronomy, 23, 39 (2009)
- [55] Laureijs, R.; et al., 2011, arXiv1110.3193
- [56] Green, J.; et al., 2012, arXiv1208.4012